1	Title:
2	Spherical Time-Encoded Radiation Imaging Simulations
3	
4	Authors:
5	John R. Kuchta <sup>a</sup> , David J. Trimas <sup>a</sup> , Peter Marleau <sup>b</sup> , David K. Wehe <sup>a</sup>
6	
7	Affiliations:
8	a) University of Michigan, Department of Nuclear Engineering and Radiological Sciences, 2355
9	Bonisteel Blvd, Ann Arbor, MI 48109, United States of America
10	b) Sandia National Laboratories, Radiation and Nuclear Detector Systems Group, 7011 East Ave,
11	Livermore, CA 94550, United States of America
12	
13	Corresponding Author:
14	John Kuchta, jkuchta@umich.edu, University of Michigan, Department of Nuclear Engineering
15	and Radiological Sciences, 2355 Bonisteel Blvd, Ann Arbor, MI 48109, United States of America
16	
17	Abstract:
18	Radiation source localization is important for nuclear nonproliferation and can be obtained using
19	time-encoded imaging systems with unsegmented detectors. A scintillation crystal can be used
20	with a moving coded aperture mask to vary the detected count rate produced from radiation
21	sources in the far field. The modulation of observed counts over time can be used to reconstruct
22	an image with the known coded aperture mask pattern. Current time-encoded imaging systems

23 incorporate cylindrical coded aperture masks and have limits to their fully coded imaging field-24 of-view. This work focuses on expanding the field-of-view to  $4\pi$  by using a novel spherical coded 25 aperture mask. A regular icosahedron is used to approximate a spherical mask. This icosahedron 26 consists of 20 equilateral triangles; the faces of which are each subdivided into four equilateral 27 triangle-shaped voxels which are then projected onto a spherical surface, creating an 80-voxel 28 coded aperture mask. These polygonal voxels can be made from high-Z materials for gamma-ray 29 modulation and/or low-Z materials for neutron modulation. In this work, we present Monte Carlo 30 N-Particle (MCNP) simulations and simple models programmed in Mathematica to explore image 31 reconstruction capabilities of this 80-voxel coded aperture mask. 32 33 Keywords: 34  $4\pi$  field-of-view, gamma-ray, nuclear nonproliferation, neutron, regular icosahedron, time-35 encoded imaging. 36 37 Abbreviations: 38 cTEI - cylindrical time-encoded imaging 39 FOV - field-of-view 40 FWHM – full width at half max GDA – Great Deluge Algorithm 41 42 MCNP - Monte Carlo N-Particle 43 sTEI - spherical time-encoded imaging 44 TEI - time-encoded imaging

1. Introduction

Imaging of radiation sources with a  $4\pi$  field-of-view (FOV) has previously been achieved with spherical arrays of detectors, both semiconductors and scintillators, and by Compton imaging [1][2]. These methods utilize pixelated detectors and/or arrays of detectors, leading to increased system cost, weight, and size. The use of radiation shielding material as the coded aperture array with only a single non-pixelated scintillation crystal is relatively inexpensive and has a simple, fast readout. This has previously been used with a rotating cylindrical coded aperture mask and an unsegmented scintillation crystal for 1D [3] and 2D [4] imaging with a limited FOV. This technique is referred to as cylindrical time-encoded imaging (cTEI). We are proposing the natural evolution to spherical time-encoded imaging (sTEI), that will increase the FOV to  $4\pi$  while retaining the simplicity of the imaging modality.

Coded aperture masks can have a variety of static patterns or be made cyclic for time-encoded imaging. For example, one ideal coded aperture pattern is the uniformly redundant array (URA) [5], but there are multiple kinds of URAs, including modified [6] and mosaic [7] URAs, and under ideal circumstances, the pattern autocorrelates a point source to a delta function. However, more random coded aperture patterns can also be used, and we discuss next a technique to choose random patterns that can perform comparably to URAs.

In previous work, we have designed cTEI masks [8] using the Great Deluge Algorithm (GDA) to pseudo-optimize random coded aperture patterns. This algorithm creates a random mask pattern of 0's and 1's and calculates a pattern quality metric [9]. It assigns the opposite value to

Commented [KJ1]: Add references

a randomly chosen mask element and recalculates the quality metric, and the voxel change is accepted if the quality metric value is sufficiently greater than the previous value. The mask pattern converges to a pinhole camera for point sources and no background radiation, and it converges to a 50% open fraction for a nominal background level and/or extended sources.

## 2. Design and Methods

73 2.1 Coded Aperture Design

Two options for tiling a spherical surface are by orthogonal polar and azimuthal segmentation (i.e., longitude and latitude lines) or by an equilateral triangle segmentation with a regular icosahedron base as seen in Fig. 1. If the spherical system is stationary and only rotates around a single axis, the polar and azimuthal segmentation could be advantageous. The segmented voxels around the opposite poles of the system would be smaller than the voxels at the equator, allowing a variable modulation of sources depending on the choice of rotation axis. However, our system is ultimately envisioned to be a freely rolling sphere with the ability to rotate around any axis. For this application, it is advantageous to have coded aperture voxels of equal shape and size. The regular icosahedron has 60 rotational natural symmetries, allowing many axes of rotation useful for image reconstruction. These natural symmetries have been utilized in chemistry for topological mapping of chemicals [10] and are being revisited here for spherical axes of rotation.

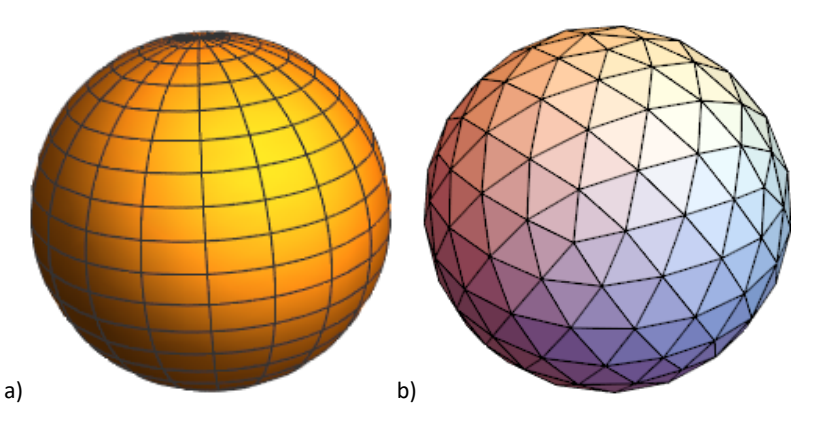


Fig. 1: The two spherical mask pattern shapes being considered: a) a polar and azimuthally segmented mask resembling a globe, b) a regular icosahedron split into smaller aperture voxels.

The GDA coded aperture optimization has been used by others to optimize the coded aperture of other  $4\pi$  imaging systems; one used a rounded 2D-cross segmented into squares [1] and another utilized the regular icosahedron [2]. Both systems used spherical arrays of detectors, but the GDA can still be used to optimize a spherical coded aperture with a central detector.

## 2.2 Validation Modeling

To simulate a sTEI system, a polygonal approximation of a spherical mask pattern was first coded in Mathematica. A regular icosahedron was created, and each of the 20 triangular faces were then subdivided twice into four smaller triangles to make the 320-element mask shown in Fig. 2. These smaller triangles were then projected onto a spherical surface to create an approximately spherical mask. The mask was chosen to have an approximately 50% open fraction and the spatial distribution of open elements on the mask was randomly selected.

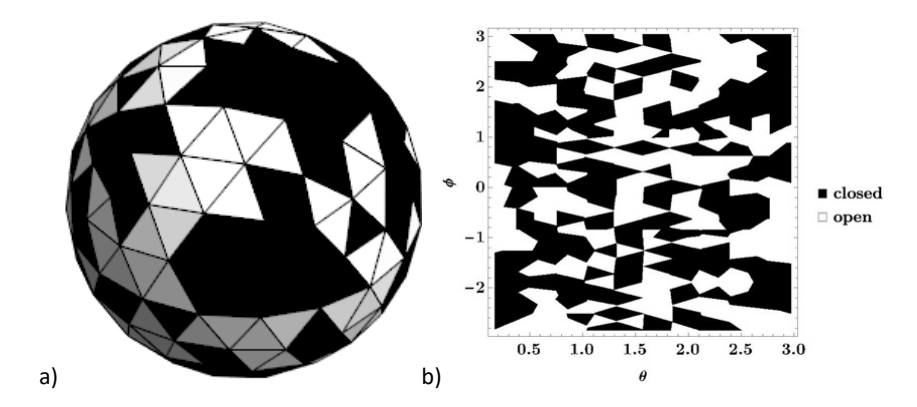


Fig. 2: Random coded aperture pattern with a segmented regular icosahedral base a) projected onto a sphere and b) plotted as a polar and azimuthally segmented mask. Closed mask elements are black, open mask elements are white.

An imaging plane was created with 5,760 imaging pixels, 18 subpixels per coded aperture voxel. The system response matrix for the spherical mask is made of 1's and 0's corresponding to the open and closed elements closest to each imaging voxel. Each row the of the system response matrix is a circulant rotation of the previous row, creating an m-by-m array where m is the number of imaging pixels. The count modulation,  $\overline{y_0}$ , for a source distribution,  $\vec{x}$ , with a sensing matrix, A, is the forward projection of  $\vec{x}$  through the sensing matrix, as shown in Eqn. (1).

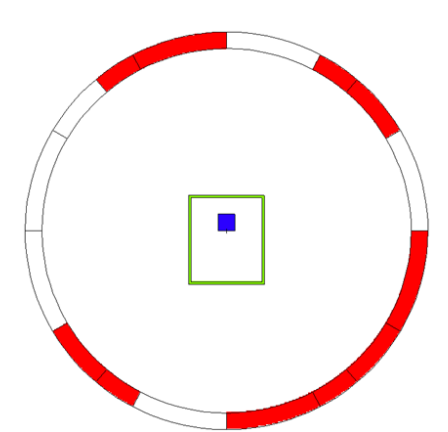
$$\overrightarrow{y_0} = A.\,\overrightarrow{x} \tag{1}$$

A source distribution was created with the same dimensions as the imaging plane. A single pixel was assigned an arbitrary intensity value of 100 and the rest were assigned a value of 10,

corresponding to a nominal background level. Maximum likelihood expectation maximization (MLEM) was used to reconstruct spatial images from the data generated by Mathematica [11]. The results will be shown in Section 3.1.

## 2.3 MCNP Simulation

MCNP6.2 was used to further simulate the radiation response of the system. MCNP is a more realistic simulation tool for radiation transport and allows for radiation scatter in surroundings to be tracked. The regular icosahedron was projected onto a sphere with more fidelity using MCNP versus the polygonal structure in Mathematica. This was made possible with ARB (arbitrary) macrobodies defining the vertices of the coded aperture mask, and then two SO (origin-centered sphere) macrobodies cut through the ARB. The intersection of all three macrobodies defines a spherically wedged coded aperture voxel. A vertical slice of the geometry can be seen in Fig. 3. Two geometries were tested for validation of the sTEI system.



135 Fig. 3: Side slice view of a sample sTEI coded aperture mask with filled voxels (red), a 136 polycarbonate light-tight box (green), and a 1-inch CLLBC scintillation crystal (blue). 137 MCNP includes the count rate artifacts produced when comparing sources in the near- and far-138 139 field. The simulations assumed a 35 cm diameter spherical mask of 80 tessellated equilateral 140 triangles. The mask pattern used was randomly generated with a 50% chance for a voxel to be open or closed. A 1-inch CLLBC scintillator [12] was simulated at the center of the mask inside 141 142 and inside a polycarbonate light-tight box. An isotropic Cs-137 point source was simulated at 3.40 143 m and 8.08 m from the sTEI mask to compare near- and far-field count rate artifacts. The source 144 was simulated at each point corresponding to a projection through the centroid of each triangle. 145 This permits simulating the sphere rotated around arbitrary axes and covering the  $4\pi$  image 146 space. 147 148 Another simulation was run for a further source distance of 8.5 m and directed as a cone at the 149 sTEI coded aperture system. Four projected source positions were used per triangle for a total 150 of 320 sources positions at the centroids of a further segmented 320-sided regular icosahedron. 151 This simulation was reconstructed using 25 iterations of MLEM to further test the imaging 152 capabilities. 153 154 To explore the advantage of multiple axes of rotation, the sTEI mask was simulated as having a 70 cm diameter and a 2.54 cm thickness of tungsten. A 1 MeV monoenergetic gamma-ray source 155 at -2-meters along the Z-axis was chosen, with a 1-inch CLLBC scintillator as the central non-156

pixelated detector. The detector cell was kept static while the random pattern spherical mask was rotated around the X-, Y-, and then Z-axis. The regular icosahedron is symmetrical around these axes, and although more axes can be simulated, there is diminishing return on image quality improvements with each additional axis. The MCNP6.2 simulations did not include the effects of background radiation, room return, pulse processing, or detector efficiency. The results in Section 3.2 only use total detector count rate, although the use of spectroscopy would further improve the simulated angular resolution. 3. Results and Discussion 3.1 Validation Modeling Results Counts were simulated in Mathematica by forward projecting the source distribution through the sensing matrix and then Poisson sampling the counts. From the data, the image shown in Fig. 4 was reconstructed using MLEM. The reconstruction pinpointed the maximum intensity pixel in the source space, validating this method as a preliminary technique for sTEI simulation. The Mathematica results are treated as qualitative, and the image resolution is constrained by the imaging plane segmentation. This method was sufficient to show MLEM images of forward projections.

157

158

159

160

161

162

163

164

165

166

167

168

169

170

171

172

173

174

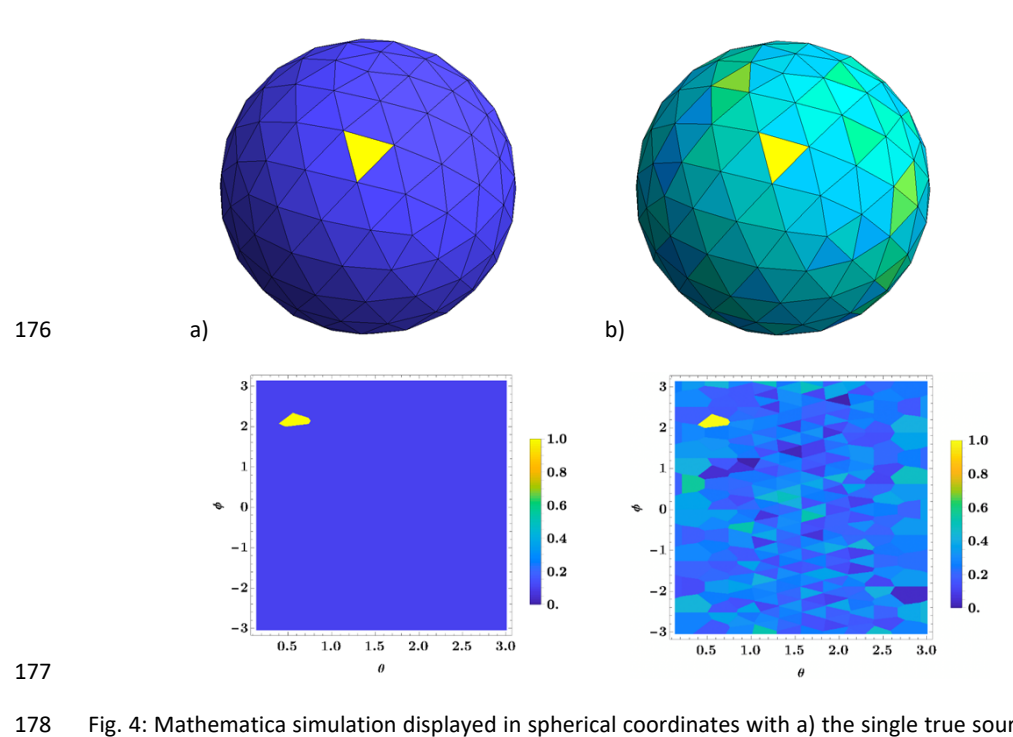


Fig. 4: Mathematica simulation displayed in spherical coordinates with a) the single true source pixel and b) the MLEM reconstruction, both normalized for qualitative view.

## 3.2 MCNP Simulation Results

MLEM was used to reconstruct an image for a source in the far field, 8.5-m from the centroid detector. This simulated source was an anisotropic Cs-137 gamma-ray cone source directed at the sTEI system. The MLEM reconstruction is seen in Fig. 5 projected onto a sphere and plotted in azimuthal and polar coordinates. The imaging resolution of this simulation is  $\sim$ 7° in azimuth and  $\sim$ 6° in the polar direction at the FWHM. This could be improved by optimizing the coded aperture mask pattern, thickness, and radius.

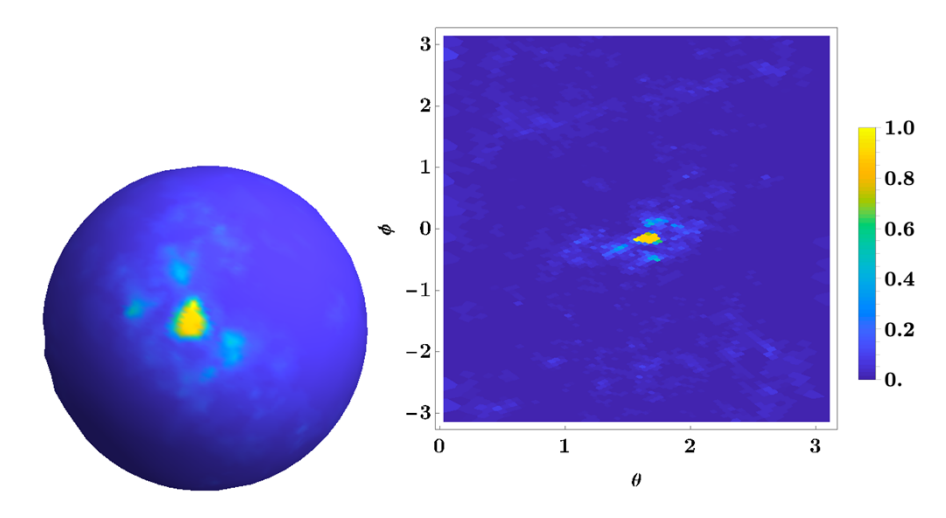
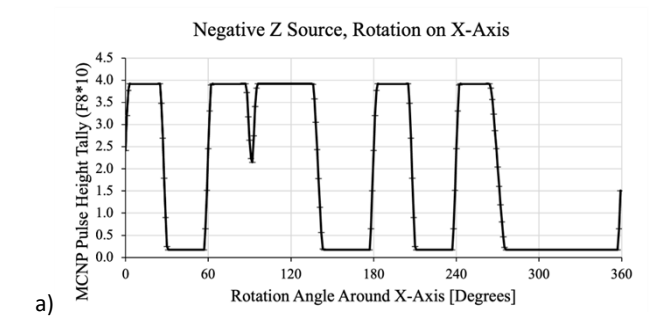


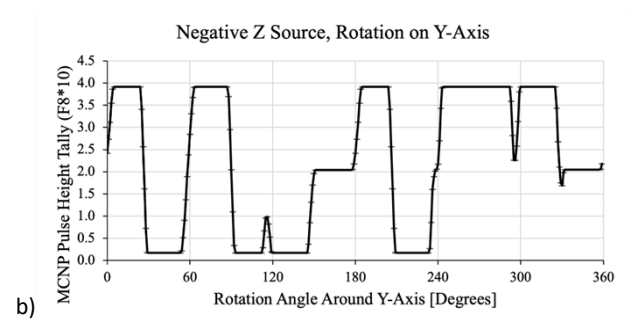
Fig. 5: A MCNP6.2 simulated Cs-137 far field source directed at the sTEI system, reconstructed using MLEM with 20 iterations.

The final sTEI simulation was designed to validate the need for multiple axes of rotation and the use of the regular icosahedron as the base geometry for sTEI. The total detector count rate modulation can be seen in Fig. 6 for the three axes of rotation with a 1-MeV monoenergetic gamma-ray source in the negative-Z direction. As expected, the tungsten mask heavily modulates the source when rotated about the X- and Y-axis, while rotation around the Z-axis should not result in the count rate changing. The MCNP6.2 output tally error is greater than the modulation bounds for the Z-axis rotation, concluding that the count rate is constant for a Z-axis rotation when the source is along the Z-axis of the system. If the system were only rotated around the Z-axis, it would be incorrectly concluded that there is no source present. The difference in count rate between the rotations around the X- and Y-axis determines that there is a source and could potentially improve imaging quality when combining the data between the two instead of using

one or the other. This is because the coded aperture mask pattern seen by the source is different

for each axis of rotation. Exploiting this effect should be done in future work.





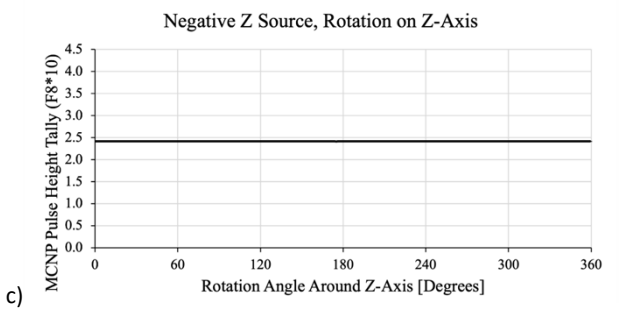


Fig. 6: The modulation of detector count rate for rotation of the sTEI system around the a) X-axis,

b) Y-axis, and c) Z-axis.

212 213 3 Conclusion 214 Spherical time-encoded imaging has been validated with simulation as a potential evolution from 215 cylindrical time-encoded imaging. The spherical coded aperture mask should be designed as a regular icosahedron due to its natural symmetries and for its ability to evenly segment each 216 217 tessellated equilateral triangle. As multiple axes of rotation become desirable, a tessellation coded aperture becomes more important for simplification of image reconstruction and should 218 219 even be advantageous. The three choices of rotation around the X-, Y-, and Z-axis allow for no 220 data to be lost along any one axis. 221 222 This simulation work should inspire new ideas and designs for  $4\pi$  imaging systems. Future work 223 could be designing a free moving sphere with a regular icosahedral coded aperture shell for advanced and adaptive imaging of radiation in the environment. 224 225 226 Acknowledgments: 227 The authors would like to acknowledge the Radiation and Nuclear Detector Systems Group at 228 Sandia National Laboratories for their collaboration and insight on this project. Sandia National 229 Laboratories is a multi-mission laboratory managed and operated by National Technology & Engineering Solutions of Sandia, LLC (NTESS), a wholly owned subsidiary of Honeywell 230 231 International Inc., for the U.S. Department of Energy's National Nuclear Security Administration

(DOE/NNSA) under contract DE-NA0003525. This written work is authored by an employee of

NTESS. The employee, not NTESS, owns the right, title and interest in and to the written work

232

and is responsible for its contents. Any subjective views or opinions that might be expressed in the written work do not necessarily represent the views of the U.S. Government. The publisher acknowledges that the U.S. Government retains a non-exclusive, paid-up, irrevocable, worldwide license to publish or reproduce the published form of this written work or allow others to do so, for U.S. Government purposes. The DOE will provide public access to results of federally sponsored research in accordance with the DOE Public Access Plan. Funding: This work was supported by Consortium for Monitoring, Technology, and Verification under Department of Energy National Nuclear Security Administration award number DE-NA0003920. References: [1] D. Hellfeld, P. Barton, D. Gunter, L. Mihailescu, and K. Vetter, "A spherical active coded aperture for  $4\pi$  gamma-ray imaging," IEEE Transactions on Nuclear Science, vol. 64, no. 11, pp. 2837-2842, 2017. [2] X. Liang, L. Shuai, Y. Liu, X. Li, L. Kong, Q. Wei, Y. Wang, Z. Zhang, X. Huang, X. Hu, Y. Zhang, Y. Yu, C. Wei, and L. Wei, "Coded aperture and compton imaging capability of spherical detector system design based on gagg scintillators: A monte carlo study," Nuclear Instruments and Methods in Physics Research Section A: Accelerators, Spectrometers, Detectors and Associated Equipment, vol. 1044, p. 167503, 2022. [3] N. P Shah, J. VanderZanden, and D. K. Wehe, "Design and construction of a 1-d, cylindrical, dual-particle, time-encoded imaging system," Nuclear Instruments and Methods in Physics

234

235

236

237

238

239

240

241

242

243

244

245

246

247

248

249

250

251

252

253

254

- 256 Research Section A: Accelerators, Spectrometers, Detectors and Associated Equipment, vol.
- 257 954, p. 161785, 2020, symposium on Radiation Measurements and Applications XVII.
- 258 [4] R. E. Krentz-Wee and P. Marleau, "Optimization of a confidante system (confirmation using a
- 259 fast-neutron imaging detector with anti-image null- positive time encoding)." Sandia National
- Lab.(SNL-CA), Livermore, CA (United States), Tech. Rep., 2019.
- 261 [5] E. E. Fenimore and T. M. Cannon, "Coded aperture imaging with uniformly redundant arrays,"
- 262 Applied optics, vol. 17, no. 3, pp. 337–347, 1978.
- 263 [6] S. R. Gottesman and E. E. Fenimore. "New family of binary arrays for coded aperture imaging".
- 264 In: Applied optics 28.20 (1989), pp. 4344–4352.
- 265 [7] E. Fenimore. "Coded aperture imaging: predicted performance of uniformly redundant
- arrays". In: Applied optics 17.22 (1978), pp. 3562–3570.
- 267 [8] J.R.Kuchta, P.Marleau, M.Sweany, D.K.Wehe, LANTERN: A Cylindrical Time-Encoded Dual
- 268 Particle Imager, in: Presentation at the 2022 IEEE Nuclear Science Symposium, Medical Imaging
- 269 Conference and Room Temperature Semiconductor Detector Conference.
- 270 [9] A. Busboom, H. Elders-Boll, and H. D. Schotten, "Combinatorial design of near-optimum masks
- for coded aperture imaging," in 1997 IEEE International Conference on Acoustics, Speech,
- and Signal Processing, vol. 4. IEEE, 1997, pp. 2817–2820.
- 273 [10] R. King and D. Rouvray. "Chemical applications of topology and group theory: 19. The even
- 274 permutations of the ligands in five-coordinate complexes viewed as proper rotations of the
- regular icosahedron [1]". In: Theoretica chimica acta 69 (1986), pp. 1–10.
- 276 [11] L. A. Shepp and Y. Vardi, "Maximum Likelihood Reconstruction for Emission Tomography,"
- 277 IEEE Transactions on Medical Imaging, vol. 1, 1982.

278 [12] P. P. Guss, T. G. Stampahar, S. Mukhopadhyay, A. Barzilov, and A. Guckes. "Scintillation

properties of a Cs2LiLa (Br6) 90%(Cl6) 10%: Ce3+ (CLLBC) crystal". In: Radiation Detectors:

Systems and Applications XV. Vol. 9215. SPIE. 2014, pp. 27–41.